communications earth & environment

Article

https://doi.org/10.1038/s43247-024-01343-5

Millennial-aged pyrogenic carbon in high-latitude mineral soils

Marcus Schiedung [1,2,3] ✉, Philippa Ascough[4], Severin-Luca Bellè [1,5], Michael I. Bird [6], Lisa Bröder [7], Negar Haghipour[7,8], Robert G. Hilton[9], Julie Lattaud [7,10] & Samuel Abiven [11] ✉

Wildfires in the Arctic are producing pyrogenic carbon as product of incomplete biomass combustion. The storage and distribution of pyrogenic carbon in soils is poorly known, especially in carbon rich permafrost-affected mineral soils. Here, we extracted pyrogenic carbon in mineral soils from eleven forest sites across the North Canadian permafrost regions by hydrogen pyrolysis. We found pyrogenic carbon with millennial-scale ages that were older in continuous (1960–12,690 calibrated years before present) than in discontinuous (510–3560 calibrated years before present) permafrost-affected soils. In all cases, pyrogenic carbon showed longer residence times compared to bulk soil organic carbon. The proportions of pyrogenic carbon on total soil organic carbon were consistent at 6.9 ± 0.5% of total soil organic carbon. Thus, pyrogenic carbon forms a significant component of the total soil organic carbon and climatic as well as soil factors control the long residence times of pyrogenic carbon in vulnerable high-latitude forest mineral soils.

Pyrogenic carbon (PyC) is considered to be an important component of the global soil organic carbon (SOC) pool[1,2]. It is naturally produced by wildfires as a product of incomplete combustion and pyrolysis of biomass[3]. Wildfires are an essential disturbance of high-latitude boreal ecosystems. Their intensity and frequency are predicted to increase with global warming, which is occurring at much faster rates in high-latitude regions and is described as Arctic amplification[4–7]. Annual PyC production is estimated to be in the range of 196–340 Tg globally and losses by decomposition are estimated to be around 89 Tg PyC annually[8,9]. When the burnt vegetation is fully re-grown, the remaining 'legacy' PyC makes wildfires a net sink of carbon. Production by pyrolysis increases the resistance of PyC to environmental degradation compared to non-pyrolyzed organic matter due to increased aromaticity by condensation[2,10,11]. The concept of a universally high persistence of PyC in soils has been challenged by field and laboratory experiments showing rapid losses of fresh PyC by mineralization on annual to decadal timescales[12–14]. However, large-scale and long-term PyC dynamics in natural soil systems have rarely been studied, especially in the high-latitude regions that cover large areas of the northern hemisphere.

High-latitude soils at >60° north store 30–40% of global SOC, and boreal forest mineral soils account for around two-thirds of this SOC pool[15–17]. In permafrost-underlain mineral soils, organic matter preservation is facilitated by cold conditions, which makes these regions particularly vulnerable to accelerated Arctic warming and permafrost thaw[4,18,19]. Slow cycling of organic matter in permafrost-affected regions result in its accumulation and aging in the soil, modulated by processes unique to high-latitude environments, such as cryoturbation and vertical mixing[20–22]. Vertical mixing by freeze and thaw dynamics transfers organic matter to greater soil depths, thereby controlling the SOC residence time in boreal mineral soils[23,24]. Longer residence times for SOC in high-latitude regions are further indicated by the release of aged dissolved organic carbon into rivers during abrupt permafrost thaw-related releases (e.g., $F^{14}C$ of 0.85 ± 0.16 corresponding to 1306 ± 1530 ^{14}C years)[25] and also aged soil-respired carbon-dioxide from high-latitude regions[26].

Studies of river water and sediments of the Mackenzie watershed, the largest watershed in Canada covering one-fifth of the national land surface, showed significant input of aged organic carbon from soils and thawing permafrost to the aquatic system together with a potential input of

[1]Department of Geography, University of Zurich, Zurich, Switzerland. [2]Department of Environmental Systems Science, ETH Zurich, Zurich, Switzerland. [3]Thünen Institute of Climate-Smart Agriculture, Braunschweig, Germany. [4]NEIF Radiocarbon Laboratory, Scottish Universities Environmental Research Centre, East Kilbride, UK. [5]European Molecular Biology Laboratory, Developmental Biology Unit, Heidelberg, Germany. [6]College of Science and Engineering, James Cook University, Cairns, QLD, Australia. [7]Department of Earth Sciences, ETH Zurich, Zurich, Switzerland. [8]Laboratory of Ion Beam Physics, ETH Zurich, Zurich, Switzerland. [9]Department of Earth Sciences, University of Oxford, Oxford, UK. [10]Department of Environmental Sciences, University of Basel, Basel, Switzerland. [11]Laboratoire de Géologie, Département de Géosciences, CNRS – École normale supérieure, PSL University, Institut Pierre Simon Laplace, Paris, France. ✉e-mail: marcus.schiedung@geo.uzh.ch; marcus.schiedung@thuenen.de; abiven@biotite.ens.fr

radiocarbon 'dead' organic carbon derived from sedimentary rock and so called petrogenic organic carbon (OC_{petro})[27–30]. Hilton et al. (ref. 28) estimated that around 70–90% of the total particulate organic matter in the Mackenzie River and its major tributaries is derived from biogenic sources with an average age of 5800 ± 80 ^{14}C years, when corrected for a contribution from OC_{petro}. Such ages are difficult to explain solely through plant-derived organic matter turnover, and it is possible that PyC contributes importantly to this highly aged pool. Yet, the age of PyC as a biogenic carbon pool in permafrost-affected soils and its distribution within the landscape has not been assessed. In addition, the stocks of PyC in high-latitude soils have only been explored in a few studies[31–33] and thus our understanding of PyC cycling on landscape scales, and as a contributor to total carbon stocks, remains largely unclear.

A major challenge is to extract and quantify PyC from the non-pyrogenic SOC pool within the soil matrix. Most methods rely on the higher persistence and energetic stability of PyC compared to the non-pyrolyzed SOC to define operational separation thresholds (e.g. thermal or chemical)[34,35]. The different operational thresholds for individual methods make it difficult to compare PyC measurements between methods due to individual ranges of the PyC continuum that are extracted and suggesting the need for a clear notation of the considered PyC[36]. Even more challenging is the estimation of PyC turnover time or age. Of the limited studies that consider PyC ages in soils, most assess the age of physically separated microscopic particles[37–39], while some consider ages extracted from bulk soil or soil fractions[40,41]. In either case, PyC age is typically reported to be centuries to a few thousand years. By contrast, PyC exported from the soil into aquatic systems, such as the Mackenzie River, can return ages of >20,000 ^{14}C years at the point of final discharge into the Arctic Ocean[42–44]. Additionally, terrestrial production of PyC tends to outpace export to aquatic systems[3,45] leading to a potential pre-aging 'bottleneck' prior to entry into the waterway. In this regard, soils are expected to play a substantial role as an intermediate reservoir of PyC[2,42,46].

We quantified PyC abundance in mineral soils within the permafrost-affected landscape of northern Canada to link the measured ages of the PyC to factors that potentially lead to intermediate storage of PyC in the boreal forest ecosystems. We measured the age and stock of PyC and bulk SOC in boreal forest mineral soils underlain by continuous (northern sites) and discontinuous to sporadic (southern sites) permafrost in the Mackenzie River catchment in northern Canada (Fig. 1). At eleven forest sites[23], we sampled the upper 0–15 cm and additionally two cryoturbated soils from these sites to 0–60 cm (Supplementary Table 1). Further, we included landscape gradients with soils sampled from top, slope and bottom positions in the northern and southern regions (see methods). All samples were derived from the active layer that was thawed in the summer 2019. We used hydrogen pyrolysis[47,48] to extract the PyC from bulk SOC, and determined the radiocarbon content (^{14}C; expressed as fraction modern $F^{14}C$) and stable isotope ($\delta^{13}C$) composition of the isolated PyC_{HyPy}. The $F^{14}C$ of PyC_{HyPy} represents a 'closed pool', made up of carbon fixed during growth of the vegetation from which the PyC_{HyPy} was subsequently formed. The ^{14}C age of PyC_{HyPy}, therefore, represents the time of plant growth, and assuming a short interval between this and the wildfire event, reflects its overall pool age in mineral soils. This does not allow direct comparison with the age of bulk

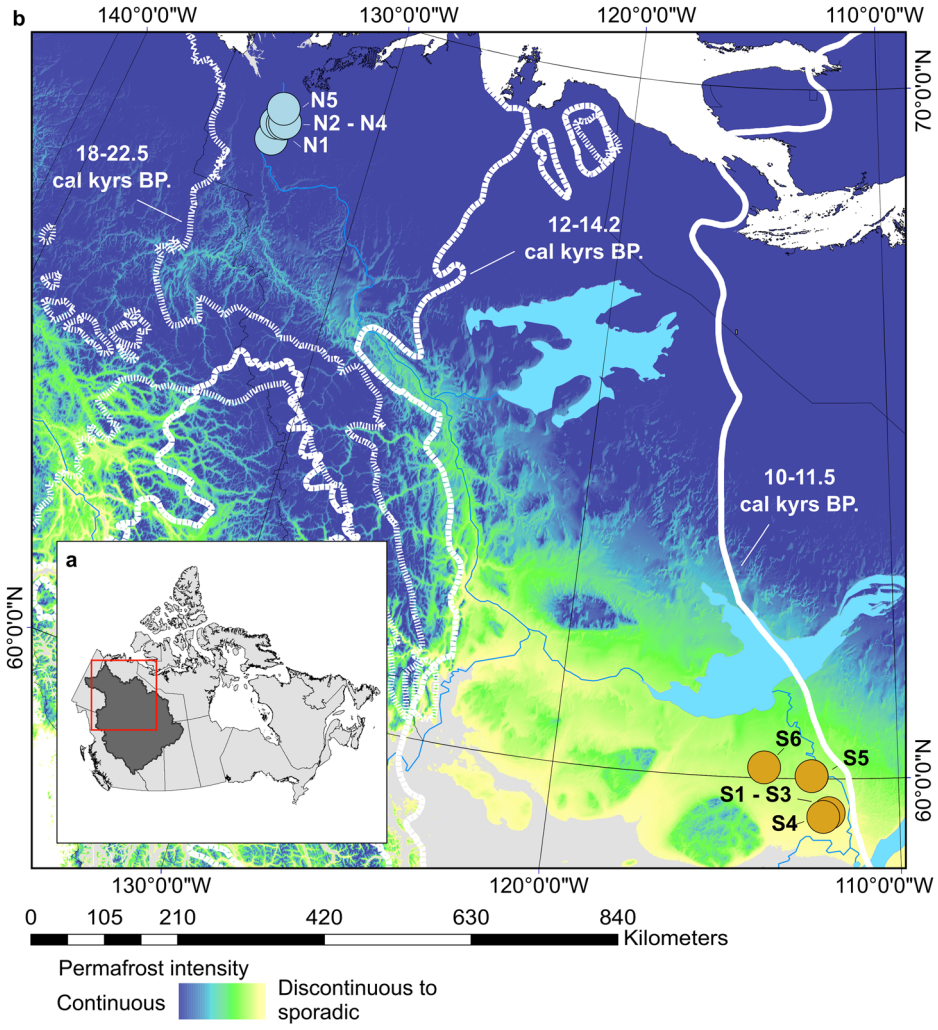

Fig. 1 | Permafrost distribution with glacial history at the study sites. a Mackenzie Catchment (dark grey area) and sampling region (red square as shown in (**b**) within the Northwest Territories and Alberta and (**b**), location of northern (N1–N5) and southern (S1–S6) sites with permafrost distribution according to Gruber (ref. 89) and glacial maximum ice-sheet extents between 10–22.5 cal. kyrs before present (BP) as presented in Dalton et al. (ref. [52]).

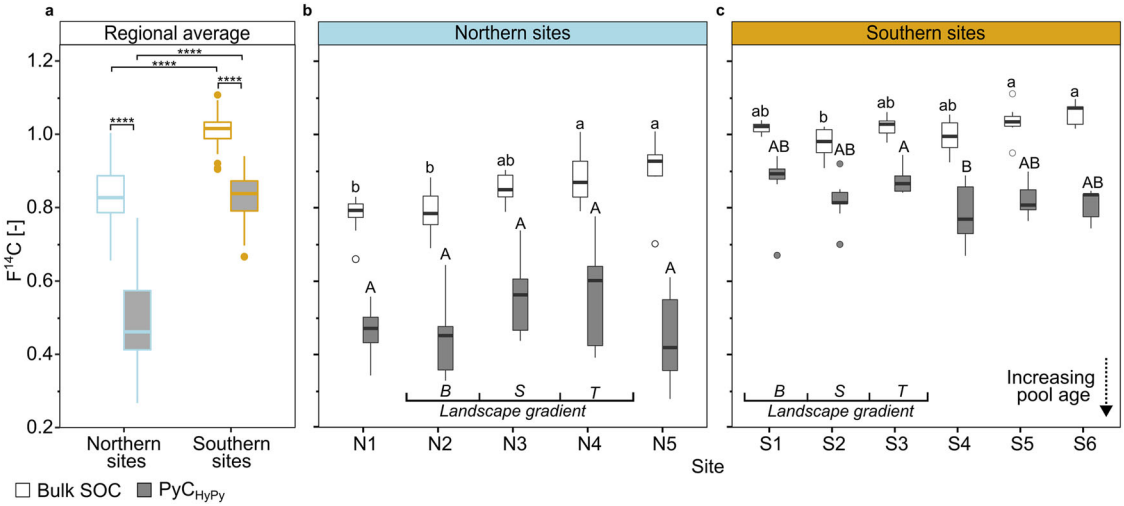

Fig. 2 | Radiocarbon activity of bulk SOC and PyC. a Bulk soil and PyC_{HyPy} $F^{14}C$ between northern and southern sites and (**b**), for individual northern and (**c**), southern sites of 0–15 cm soil depth. The landscape gradients are indicated with bottom (B), slope (S) and top (T) sites (see methods). Significant differences between northern and southern sites ($p < 0.001$, two-sided Students's t test) are indicated by asterisk and for bulk SOC (small letters) and PyC_{HyPy} (capital letters) between the individual sites within northern and southern sites ($p < 0.05$, tested with an one-way analysis of variances (ANOVA) and multiple comparison with a post-hoc-test (Tukey; 95% pairwise confidence level) and Bonferroni adjustment. In (**a**), the bulk SOC $F^{14}C$ values are composed of $n = 45$ and $n = 49$ samples for northern and southern sites, respectively. For the PyC_{HyPy}, $n = 43$ for northern and $n = 46$ for southern sites were considered. Calibrated PyC_{HyPy} ages are presented in Table 1. For all individual $F^{14}C$ values and $\Delta^{14}C$ values and number of samples per site ($n = 5$–9) see Supplementary Table 2. All boxplots show the upper and lower quantile and the median. The statistical test results are shown in Supplementary Tables 9, 10.

soil SOC. Bulk soil SOC ^{14}C measurements, in comparison, represents an 'open' pool, including components from the time of sampling (e.g. living organisms in exchange with the atmosphere at the time of sampling) as well as transient and slow cycling or stabilized SOC (including PyC) components[49].

Results and discussion

Centennial to millennial pyrogenic carbon cycling

The PyC_{HyPy} pool had consistently lower $F^{14}C$ values than the bulk SOC in the surface soils at all sites (Fig. 2, Supplementary Tables 2, 3). This underscores the longer residence time of PyC_{HyPy} compared to bulk SOC and non-pyrolyzed organic matter[10]. The differences were more pronounced in the northern continuous permafrost soils ($F^{14}C$ of PyC_{HyPy} by 0.34 ± 0.15 lower than bulk SOC $F^{14}C$) than in southern discontinuous permafrost soils ($F^{14}C$ of PyC_{HyPy} by 0.18 ± 0.10 lower than bulk SOC $F^{14}C$; Supplementary Tables 2, 3). For the two regions, the $F^{14}C$ of both PyC_{HyPy} and bulk SOC was significantly lower at the northern than southern sites ($p < 0.001$; Fig. 2a). This corresponds to a time since formation of PyC_{HyPy} that was on a centennial to millennial timescale, ranging between 1940 and 12,590 cal. yrs before present (BP) for northern and 510–3560 cal. yrs BP for southern sites (Table 1).

The observed age differences between the northern and southern permafrost regions can be explained by (i) the slower turnover of organic matter at lower temperatures in northern continuous permafrost conditions, generally resulting in high radiocarbon ages of bulk SOC within the frozen permafrost parts[22,50,51] and (ii) distinct differences in glacial history of the northern and southern soils.

The retreat of the Laurentide Ice Sheet occurred in the northern Mackenzie region around 18,000–14,200 cal. yrs BP and so the northern sites started to become ice-free at this time (Fig. 1). The southern sites started to be ice-free only by the early Holocene, around 11,500 cal. yrs BP, but remained covered by the glacial Lake McConnell until around 3500 cal. yrs BP[52,53]. Additionally, the millennia between the retreat of the Laurentide Ice Sheet and the start of the Holocene (from 15,000–11,000 yrs. BP) saw temperatures in high-latitude areas increase by an estimated 5 °C[54,55]. These higher temperatures promoted plant growth, thereby altering fuel loads and wildfires occurrence in the Holocene[54,55]. Large and intense wildfires during the warm and dry periods of the early Holocene compared to smaller fires during wetter conditions of the later Holocene,[56–58] could have resulted in significantly higher inputs of PyC into the soils at that time, that now represent a legacy contribution to the recent PyC pool.

Table 1 | Calibrated PyC_{HyPy} ages

Site	Depth	Calibrated PyC_{HyPy} age	$F^{14}C$ of PyC_{HyPy}
	[cm]	[cal. yrs BP]	[–]
N1	0–15	5329–9884 (9)	0.46 (0.02)
N2	0–15	3728–10,274 (8)	0.44 (0.04)
	15–30	7976–9541 (2)	0.34–0.41
	30–45	7906–17,796 (2)	0.16–0.41
	45–60	12,963–12,971 (2)	0.25 (0.04)
N3	0–15	2430–7669 (9)	0.56 (0.04)
N4	0–15	1942–8536 (9)	0.54 (0.05)
N5	0–15	4418–12,590 (7)	0.44 (0.05)
	15–30	25,955–26,719 (1)	0.06 (0.01)
	30–45	25,750–26,260 (1)	0.07 (0.01)
S1	0–15	513–3558 (7)	0.86 (0.04)
S2	0–15	651–3147 (9)	0.82 (0.02)
S3	0–15	509–1350 (8)	0.88 (0.01)
S4	0–15	793–3561 (6)	0.76 (0.03)
S5	0–15	731–2310 (8)	0.82 (0.01)
S6	0–15	1283–2677 (5)	0.80 (0.02)

Minimum and maximum range on a 95% confidence interval of calibrated ages of all replicates per site and depth increment. Calibration was performed using OxCal v4.4.2[84] by using the IntCal20 international calibration curve[85] (methods). The number of replicates is reported in brackets. All calibrations and age probabilities for individual samples are presented in Supplementary Fig. 1. Average $F^{14}C$ values (as range when $n = 2$ and with analytical error when $n = 1$) with one standard deviation corresponding to the calibration ages. All values of the bulk SOC are presented in Supplementary Table 2.

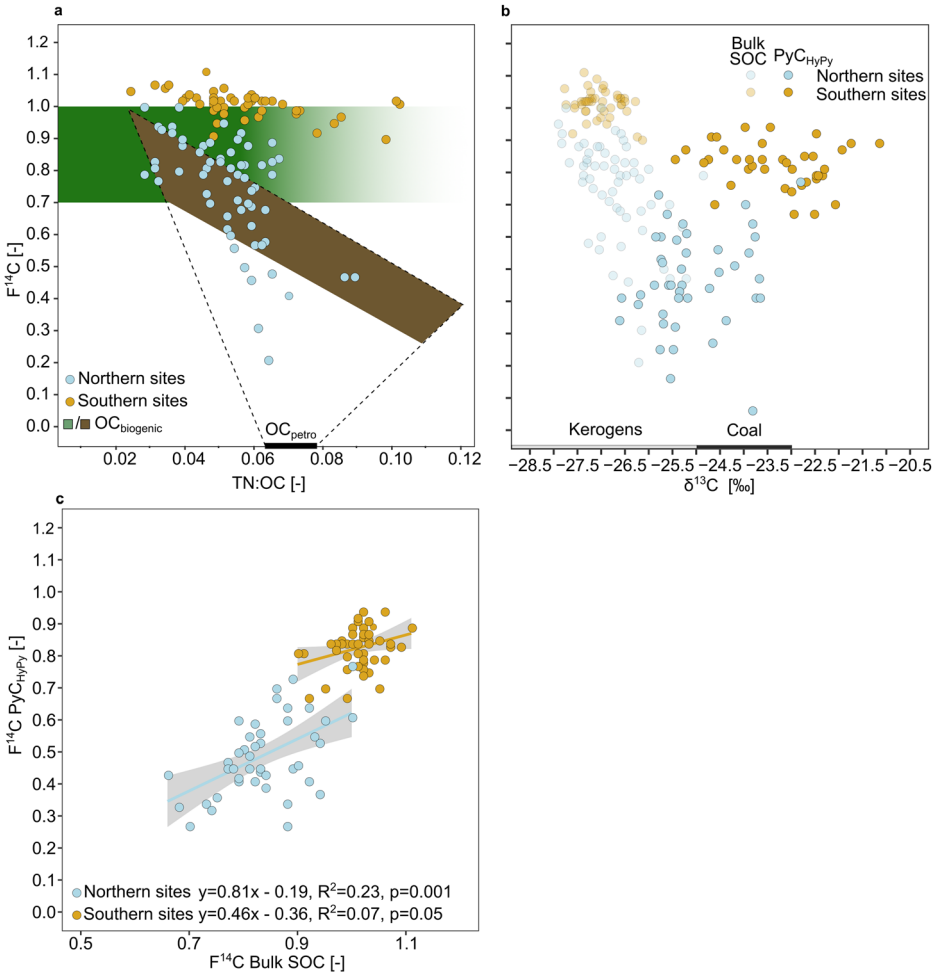

Fig. 3 | Source of bulk SOC and isotopic shifts of PyC_{HyPy}. **a** Measured bulk soil $F^{14}C$ versus the total nitrogen to organic carbon ratio (TN:OC) with $F^{14}C$ range of long-chain fatty acids ($C_{28\text{-}30}$) measured in northern soils (Supplementary Table 3; green shaded area) and expected composition of OC_{petro} (black rectangle) and $OC_{biogenic}$ (brown shaded area) as reported for particulate organic carbon in major rivers of the Mackenzie River watershed and western Canadian peat core with expected mixing of biogenic and petrogenic C reported by Hilton et al. (ref. 28). **b** Shift in stable $\delta^{13}C$ isotope composition from bulk soil and PyC_{HyPy} with expected $\delta^{13}C$ ranges of kerogens as grey bar (kerogens I-III; −35 to −25‰) and bituminous coal as black bar (−25 to −22‰) from a global assessment[90]. **c** Relation between $F^{14}C$ of bulk SOC and $F^{14}C$ of PyC_{HyPy} with linear regression for northern and southern sites. Further discussion on petrogenic contribution is presented in Supplementary Texts 1, 2.

In cryoturbated northern soils, the $F^{14}C$ values further decreased with increasing soil depth below 15 cm for both bulk SOC and PyC_{HyPy} (Supplementary Fig. 2). The decrease in bulk SOC $F^{14}C$ was more pronounced in soils located at elevated landscape positions and less pronounced with depth in extensively cryoturbated moist, silt- and ice-rich lowland sites (Supplementary Tables 1 and 3)[23,24]. At soil depths below 15 cm, the ages of PyC_{HyPy} ranged from 7906–26,719 cal. yrs. BP (Table 1).

These old ages can be partly explained by relative accumulation and enhanced stabilization of PyC at greater soil depths[59–61] with consequent increases in residence times. However, the oldest PyC_{HyPy} ages exceed the time of the ice sheet retreat, indicating that some extracted PyC_{HyPy} might be influenced by PyC produced during interglacial periods or geological OC_{petro}, either of which would exceed the maximum age of radiocarbon dating (e.g. >50,000 ^{14}C years; radiocarbon 'dead') and consequently lower the $F^{14}C$ values.

The Mackenzie catchment is located in the Western Canada Sedimentary Basin and potential sources of OC_{petro} are immature bitumen, coal and sedimentary rock such as shales from the Devonian Canol Formation[62,63]. The assessment of bulk soil TN:SOC ratios indicated a mixing of OC_{petro} and biogenic organic carbon ($OC_{biogenic}$) in northern bulk SOC based on reported compositions of peat-derived OC in the Mackenzie River catchment and plant-derived long-chain fatty acids ($C_{28\text{-}30}$) extracted in this study (Fig. 3a)[25,28,64]. Long-chain fatty acids with similar $F^{14}C$ (0.70–1.00; Supplementary Table 3) compared to the bulk SOC in 0–15 cm at northern sites showed that the bulk SOC is predominantly composed of plant-derived OC. However, at greater soil depth at the northern sites (N2 and N5), the fatty acids showed lower $F^{14}C$ values ($F^{14}C$ of 0.70–0.73) compared to the bulk SOC ($F^{14}C$ of 0.06–0.25). This points to an increased contribution of radiocarbon 'dead' compounds such as OC_{petro} with increasing soil depth[65]. The southern sites indicated no clear influence by OC_{petro} when considering the TN:SOC composition and $F^{14}C$ signatures of plant derived endmembers and are, therefore, most likely dominated by post-last glacial biogenic organic matter.

The $F^{14}C$ of bulk SOC in 0–15 cm at the northern sites would shift by 5–17% towards higher $F^{14}C$, and therefore younger ages, as a result of mixing with OC_{petro} (see Supplementary Text 1). Estimating the proportion of OC_{petro} in PyC pools is particularly difficult due to the chemical overlap of the biogenic PyC and OC_{petro} compounds (see Supplementary Text 2 and ref. 48). By comparing the $\delta^{13}C$ values of bulk SOC and PyC_{HyPy} versus $F^{14}C$ of northern sites, the potential influence of OC_{petro} can be assessed similarly to bulk SOC (Fig. 3b). A significant contribution of OC_{petro} derived from organic matter rich sediments (e.g. coal deposits or black shales) would most likely not be homogeneously distributed due to its origin as particles and small clasts and result in much larger variability of $F^{14}C$ between samples. However, all measured PyC_{HyPy} in 0–15 cm had low $F^{14}C$ values ($F^{14}C < 0.77$; Fig. 2) and the absence of any PyC_{HyPy} value reaching more modern $F^{14}C$, compared to southern sites (e.g. >0.80), supports the interpretation that the biogenic PyC pool in the continuous permafrost-affected northern soils is much older than in soils overlying the discontinuous to sporadic permafrost at the southern sites. The dominance of biogenic PyC in the extracted PyC_{HyPy} fraction is further supported by similar relationships between bulk SOC $F^{14}C$ and PyC_{HyPy} $F^{14}C$ in northern and southern sites (Fig. 3c). Nevertheless, the presence of OC_{petro} in soils should be further considered in future research to determine effects on estimated residence times of PyC and SOC components[66].

Vonk et al. (ref. 67) reported bulk organic carbon ages for sediments of the Mackenzie Delta region of up to 12,000 ^{14}C yrs, but estimated an OC_{petro} contribution of 19 ± 9%, which resulted in $OC_{biogenic}$ ages of 6100 ^{14}C yrs, which is comparable to 5800 ± 80 ^{14}C years estimated by Hilton et al. (ref. 28). The PyC_{HyPy} extracted from the soils in this study showed similar radiocarbon signatures to the ages reported for particulate organic carbon and black carbon exported from the Mackenzie River (here $\Delta^{14}C$ of −131 to −933‰, Supplementary Table 2; compared to $\Delta^{14}C$ of −738 to −856‰)[68]. This highlights the fact that PyC derived from wildfires is undergoing substantial pre-aging through storage in boreal forest mineral soils, resulting in millennial ages even in near-surface soils. Our results show that the PyC pool in permafrost-affected soils may contain significant amounts of PyC produced during post-glacial and early Holocene wildfires rather than being dominated by inputs from more recent wildfire activity. This in turn indicates that fresh PyC inputs might cycle faster under current conditions[12] than the ancient PyC pool that is dominating the contribution to overall PyC age in permafrost-affected soils.

Pyrogenic carbon is a consistent fraction of soil organic carbon

The contribution of PyC_{HyPy} to total SOC (PyC_{HyPy}/SOC%) was 6.9 ± 0.5% on average for all sites in 0–15 cm depth, with no difference between northern and southern sites ($p = 0.83$; Fig. 4a; Supplementary Table 2). Despite the similar average proportion, the minimal and maximal values indicated a substantial range (0.8–26.3 PyC/SOC%) and therefore large spatial variability in PyC distribution in boreal forest mineral soils (Supplementary Fig. 3). The absolute PyC_{HyPy} contents were higher at northern than at southern sites ($p < 0.01$; Fig. 4b), equating to four times higher SOC contents in the northern soils[23]. As a result, the PyC_{HyPy} stocks over 0–15 cm at northern sites (3.4 ± 0.3 Mg PyC_{HyPy} ha^{-1}) were twice than those of southern sites (1.4 ± 0.1 Mg PyC_{HyPy} ha^{-1}; $p < 0.01$; Fig. 4c, d), but the differences between sites were less pronounced than for SOC due the higher variability in PyC_{HyPy}.

Our findings compare well with reported PyC contents of 8% of total SOC (range of 4–14% PyC of total SOC) found in the upper 0–5 cm of boreal forest soils of interior Alaska[32,69]. Similar ranges of 0.6–5.7% PyC of total SOC were reported in Siberian boreal and tundra forest soils[31,33]. However, these studies used different analytical methods to separate the PyC from bulk SOC, which may result in substantial differences in estimates of the quantified PyC pool, depending on the operationally analysed fraction of the PyC continuum[36]. This can be by physical particle separation, chemical and thermal extraction of highly condensed PyC by oxidation of the non-pyrogenic organic matter, or compound specific PyC methods. The hydrogen pyrolysis has been shown to capture most of the PyC continuum present in soils and only remove the most labile (less condensed) fraction[47]. In any case, high-latitude mineral forest soils appear to contain consistently less PyC than the global estimate of 14% PyC of total SOC[1]. Moreover, its distribution as a proportion of total SOC seems to be consistent in mineral soils across many boreal forest ecosystems at least in the near-surface soil.

The PyC_{HyPy}/SOC% increased with soil depth (Supplementary Fig. 4). We extracted the most refractory PyC pool by using chemical-thermal oxidation at 375 °C (PyC_{CTO}) to further examine trends with soil depth. The PyC_{CTO}/SOC% nearly doubled for all southern sites and along the landscape gradient at dry northern sites (N3-N5) at top positions between 0–15 cm and 15–30 cm depths. This supports the concept of a relative enrichment of PyC as a proportion of the total SOC with soil depth due to its enhanced persistence[61,70] and stronger retention by mineral surface interactions compared to non-pyrolyzed organic matter in subsoils[59,71]. Such an effect is further supported by the older ages of PyC_{HyPy} found in the subsoil (>15 cm depth), even though the presence of OC_{petro} might cause large uncertainty. In highly cryoturbated soils (N1 and N2), the SOC/PyC_{CTO}% and PyC_{HyPy}/SOC% remained constant with depth as observed for SOC, which underscores the importance of cryoturbation in determining the fate of PyC in high-latitude mineral soils (Supplementary Fig. 4). Ongoing permafrost thaw and development of thermokarst erosional features can rapidly expose deep mineral soils[66], and understanding the fate of the PyC pool in mineral soils with depth is important to understand the net carbon cycle impacts of permafrost thaw.

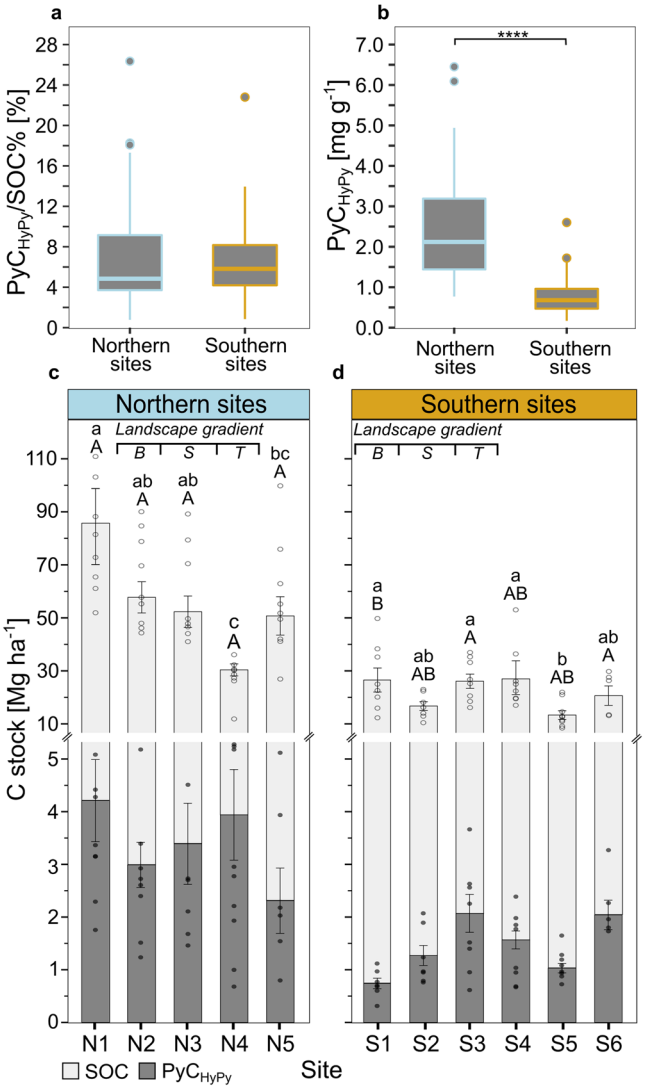

Fig. 4 | Quantity of pyrogenic carbon in soils. a Content of PyC_{HyPy} as proportion of total SOC, PyC_{HyPy}/SOC% and (**b**), as absolute contents per mass soil. Significant differences between northern and southern sites ($p < 0.001$, two-sided Student's t test) are indicated by asterisk. **c** Stocks of SOC and PyC_{HyPy} for northern and (**d**), southern sites in 0–15 cm soil depth, with standard error of the mean. The landscape gradients are indicated with bottom (B), slope (S) and top (T) sites (see methods). Capital letters indicate significant differences between PyC_{HyPy} stocks and small letters indicate significant differences in SOC stocks within northern and southern sites tested with an one-way analysis of variances (ANOVA) and multiple comparison with a post-hoc-test (Tukey; 95% pairwise confidence level) and Bonferroni adjustment. Individual data points are indicated by grey circles for SOC stocks and grey dots for PyC_{HyPy} stocks and all values and the number of samples (n = 5–9) are presented in Supplementary Table 2 and Supplementary Fig. 3. All boxplots (**a**, **b**) show the upper and lower quantile and the median. The statistical test results are shown in Supplementary Tables 11, 12.

Climate, landscape and soil properties control ages and stocks of PyC

The major differences between the northern and southern sites were climate-related permafrost conditions and glacial landscape history (Fig. 2a). At the landscape level, the F^{14}C of the PyC_{HyPy} from the northern

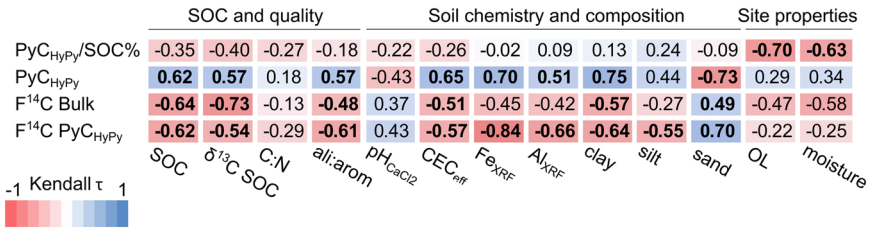

Fig. 5 | Controlling factors of PyC$_{HyPy}$ and bulk SOC age. Kendall correlation (τ) of PyC$_{HyPy}$/SOC%, PyC$_{HyPy}$ content, F^{14}C Bulk and F^{14}C PyC$_{HyPy}$ with total SOC content, its δ^{13}C, C:N ratio, aliphatic:aromatic composition of SOC determined by mid-infrared spectroscopy (ali:arom), pH determined in 0.01 M $CaCl_2$ (pH$_{CaCl2}$), effective CEC (CEC$_{eff}$), total Fe and Al determined by XRF (Fe$_{XRF}$, Al$_{XRF}$), texture as clay, silt and sand, the organic layer thickness at time of sampling (OL) and site moisture classified as dry (1), moist (2) and wet (3) as a property of soil texture, landscape position and permafrost as described by ref. 91 All values in bold are significant with $p < 0.05$ (Supplementary Table 13). All site values are presented in Supplementary Tables 1 and 5, and individual correlations are presented in Supplementary Figs. 5–8.

sites indicated no significant differences between landscape positions over the 0–15 cm interval (Fig. 2b). The bulk SOC, however, showed significantly lower F^{14}C values (older SOC) at the moist lowland sites (N1-N2) compared to dry and elevated sites (N4-N5). The lowland sites might represent forested remnants of Pleistocene ice-rich, so-called, Yedoma complexes and flood plains. Such formations consist of periglacial sediments containing around 2% organic carbon and are strongly influenced by cryoturbation[23,72]. Our results are in accordance with previous observations of site moisture being the main controlling factor of SOC preservation in the same soils[23]. At drier sites, the cycling of fresh and recent organic matter is inhibited, shifting the bulk SOC towards higher F^{14}C values, while favourable conditions at the moist sites facilitate the decomposition of fresh organic matter[12,23]. Consequently, the remaining SOC with lower F^{14}C values shows an accumulation of older organic matter. This interpretation is supported by a negative correlation between site moisture and bulk SOC F^{14}C and consequent lower F^{14}C values with increasing moisture across all sites (Fig. 5).

Generally, the variability in F^{14}C of PyC$_{HyPy}$ was lower at southern sites compared to northern sites (Fig. 2). This results in a much more homogeneous age distribution for the PyC in less permafrost-affected soils. The differences in F^{14}C between landscape positions were less pronounced for the PyC$_{HyPy}$ compared to the bulk SOC, with only two sites (S3 and S4) showing significant differences with lower F^{14}C values at the lowland site (S4; Fig. 2c).

The PyC$_{HyPy}$/SOC% showed a strong negative correlation with the organic layer thickness and site moisture (Fig. 5), where thinner organic layers and lower site moisture resulted in higher PyC$_{HyPy}$/SOC%. A similar effect of organic layer thickness on the contribution of PyC to total SOC was also found in boreal forests of interior Alaska[32], pointing towards similar controlling mechanisms. Such effects might be associated with full combustion of the organic layer and partial combustion of surface SOC during fires, compared to lower penetration of fire influence at moist sites with thicker organic layers[73]. At the same time, the accumulation of thicker organic layers might prevent the input of PyC into the mineral soil and thereby decrease PyC$_{HyPy}$/SOC% due to relative higher non-pyrogenic organic matter inputs.

The absolute PyC$_{HyPy}$ contents were mainly controlled by soil chemical properties and texture as well as SOC contents and composition. PyC$_{HyPy}$ contents were higher when the SOC was less decomposed and slower-cycling (e.g. higher δ^{13}C values, larger proportion of aliphatic to aromatic compounds and higher C:N). Preservation due to pedo-climatic conditions that constrain decomposition might thus result in larger absolute PyC$_{HyPy}$ stocks. At the same time, PyC$_{HyPy}$ contents correlated positively with total Fe$_{XRF}$ and Al$_{XRF}$ as well as clay and silt contents (Fig. 5). This highlights that stabilization at the soil mineral surfaces is an important mechanism for PyC accumulation in mineral soils[74]. Such interactions can take place as direct sorption to mineral surfaces, even resulting in desorption of non-pyrolyzed SOC or PyC acting as an aggregation agent with consequent physical occlusion[12,74,75]. This stabilization increases the long-term persistence of PyC, which is highlighted by a strong correlation between most soil chemical and compositional parameters (e.g. Fe$_{XRF}$, Al$_{XRF}$, clay and silt content) and the F^{14}C of PyC$_{HyPy}$. Given the long-term history and old ages of PyC in this study, large-scale changes in fire regime and associated differences in overall PyC input cannot be fully excluded. It is important to note that our interpretation here relies on correlations with site and soil-specific parameters, across a large gradient of permafrost conditions (Fig. 5). While it is a valuable way to consider a large range of ecosystem properties, more comprehensive studies with more specific focus on mechanistic understanding are needed to evaluate the main drivers of PyC stability in permafrost-affected soils.

Nevertheless, we show that, in permafrost-affected environments, PyC stabilization is due not only to specific landscape characteristics but also to soil properties. In a companion study investigating the persistence of fresh PyC at the same sites over two years, a potential lower PyC persistence in nutrient-limited permafrost-affected soils was observed, which was attributed to a potential for PyC to act as a nutrient source[12]. In similar boreal ecosystems, PyC was shown to speed up the cycling of non-pyrolyzed organic matter and so the decomposition of organic layers in forests[76,77], an important carbon reservoir in the boreal ecosystem[23]. In consequence, the predicted changes with global warming and Arctic amplification[78], which not only includes higher temperatures but also shifts the composition and functioning of boreal ecosystems, will impact several of the factors controlling PyC ages and stocks.

We show that PyC in high-latitude soils represents a major and consistent fraction of the total SOC that can be of millennial age. In this regard not only more mechanistic understanding is needed but also large-scale assessments by modelling are required to estimate future and globally important impacts of shifts in the PyC cycle in soils of the high-latitude regions.

Material and methods

Study sites and soil sampling

Eleven boreal forest sites were sampled within the Boreal and Taiga Plain of Northern Canada in the Mackenzie River region (Fig. 1 and Supplementary Table 1) as presented by Schiedung et al. (ref. 23). Two distinct permafrost regimes were targeted: Northern sites (N1-N5; >68° latitude north) with continuous permafrost and southern sites (S1–S6; 59–60° latitude north) with discontinuous to sporadic permafrost. Northern sites were located near Inuvik and under a subarctic ecoclimate (mean annual temperature: −9.5 °C and mean annual precipitation: 200–300 mm) with active layer depths at the time of sampling (July–August 2019) of 10–60 cm. The sites N1-N4 were located in the Great Bear Lake Plain dominated by fine-textured glacial and outwash deposits on Cretaceous shale and Devonian limestone. The sites N2-N4 were located on the Campbell Uplift, which is characterized by colluvial deposits. These sites were arranged on a landscape gradient towards Campbell Lake (580 m length, 50–90 m a.s.l. and a maximum slope of 15°), with N2 bottom, N3 slope and N4 top. The site N5 was located in the Mackenzie Delta Region on an uplift close to the Inuvik weather station. The southern sites (S1-S6) were characterized by sub-

humid mid-boreal ecoclimate (mean annual temperature: −2 °C and mean annual precipitation: 300–400 mm). The sites S1-S5 were located in the Boreal Plain of the Slave River Lowlands dominated by sandy alluvial and aeolian deposits on Palaeozoic carbonate formations. The sites S1-S3 were located on a landscape gradient towards the Pine Lake, a sinkhole in the Wood Buffalo National Park (170 m length, 270–290 m a.s.l. and a maximum slope of 12°). The site S4 was located near a degraded peatland. Site S5 was located on a periglacial dune and site S6 was located in the Hay River Lowlands, representing the transition zone between the Boreal and Taiga Plain. The landscape gradients were sampled to study potential transfer processes of PyC within the landscape. The dimension of the gradients differed between northern and southern sites (see above) as well as the aspect (northern sites: south-west and southern sites: north-east). The general climatic differences between northern and southern sites were considered to be too large to consider specific macroclimatic differences, which would have required several gradients within each region.

Soil samples were taken in July and August 2019 in a grid of 30 × 30 m, with pit sampling was performed on a raster grid, resulting in nine sampling points at each site (eight at S1 and five at S6) and 94 pits. Pits were excavated by hand to a total depth of 60 cm. Soil samples were taken using stainless-steel cores (5 cm diameter and 12 cm length) at the centre of 15 cm depth increments resulting in 0–15, 15–30, 30–45 and 45–60 cm. Three cores were composited per pit location and depth. Undisturbed samples (100 cm^3 cores) were taken from each pit and depth for bulk density estimation.

Sample preparation and analyses

Undisturbed soil samples for bulk density estimation were dried at 105 °C to constant weight. To determine the fine soil bulk density, the samples were sieved to <2 mm and larger rock and root fragments were weighed. The bulk densities were corrected for rock and root fragments to calculate stocks as described by Schiedung et al. (ref. 23). The core samples taken from the pits were air-dried and for homogenization sieved to <8 mm. Aliquots of each sample, to reduce the sample mass of 1–2 kg taken in the field, were dried at 40 °C and sieved to <2 mm for further analyses.

To obtain SOC contents, all soils with pH >6 were decarbonated using the HCl fumigation approach as described by Walthert et al. (ref. 79). This appeared in all samples from the southern sites (S1-S6). In brief, 1% HCl solution (5 µl) was added to the samples in silver cups (5 × 9 mm) and exposed to 37% HCl vapour for eight hours, followed by drying for four days under vacuum. To ensure efficient carbonate removal, shifts in $\delta^{13}C$ to more negative values were examined. All samples were milled and SOC contents and $\delta^{13}C$ values, relative to the international Vienna Pee Dee Belemnite (VPDB) standard, were determined by a dry combustion module cavity ring-down spectroscopy system (G2101-i Analyzer, Picarro, Santa Clara, USA).

Pyrogenic carbon extraction

The PyC was extracted from the soils using hydrogen pyrolysis (HyPy), hereafter PyC_{HyPy}, according to a modified approach presented by Ascough et al. (ref. 47). Dried and <2 mm Soil samples (3–4 g) were decarbonized using 1 M HCl and treating at 80 °C for a minimum of two hours on hot plates. Afterwards, the samples were filtered on a vacuum filtration system using pre-combusted 0.45 µm glass fibre filters and rinsed with deionized water to neutralize the sample. After drying, 5 wt% of fresh synthesized HyPy catalyst (ammonium dioxy-dithiomolybdate $[(NH_4)_2MoO_2S_2]$) was added to each sample. The catalyst was precipitated on the surface of the sample particles by first dissolving in a solution of 20% methanol in deionized water on a hotplate (80 °C) for a minimum of two hours. Remaining moisture was removed by freeze drying. The catalyst-loaded samples were weighed into pre-combusted quartz crucibles for HyPy treatment. The samples were pyrolyzed at 550 °C under a H_2 pressure of 150 bar and sweep gas flow of 5 L min^{-1}. The HyPy programme followed that described in Meredith et al. (ref. 48). In brief, samples were pyrolyzed by first heating from 50 °C to 250 °C (300 °C per min), and then heating to 550 °C at 8 °C per min. Samples were kept at 550 °C for 2 min and then cooled. Weight loss during HyPy was recorded, and the PyC_{HyPy} was obtained by using an elemental analyser (EA), coupled to an isotope ratio mass spectrometer (IRMS).

The most refractory PyC pool was measured by using chemo-thermal oxidation (PyC_{CTO}) following an adapted protocol presented by Agarwal and Bucheli (ref. 80). Briefly, 40 mg of milled soil were combusted at 375 °C in silver capsules for 24 h under an O_2-atmosphere in a combustion oven followed by an acid fumigation presented by Walthert et al. (ref. 79). Similar to the SOC, all PyC_{CTO} was determined by a dry combustion cavity ring-down spectroscopy system (G2101-i Analyzer, Picarro, Santa Clara, USA).

Fatty acid extraction

Dried and <2 mm sieved soil samples of site N1-N5 were additionally freeze dried and 45 g were extracted with an EDGE system (CEM) as described in Lattaud et al. (ref. 81). Following extraction, the total lipid extract was saponified with 0.5 M KOH in MeOH and the neutral fraction was liquid-liquid extracted three times with hexane. The remaining saponified products were acidified (pH ~ 1) and fatty acids were liquid-liquid extracted three times with hexane:dichloromethane (DCM) (4: 1, v/v). The acid fraction was then methylated overnight (12 h, 70 °C) with MeOH: HCl (95: 5, v/v) of known isotopic composition, and the resulting fatty acid methyl esters (FAMEs) were liquid-liquid extracted four times with hexane. FAME quantification using GC-FID has been described in Lattaud et al. (ref. 81). To quantify the compounds, a known amount of C_{36} n-alkane was run multiple times as external standard during the same sequence.

Radiocarbon measurement

The radiocarbon analyses of the PyC_{HyPy} and bulk soil samples were performed on individual 0–15 cm samples from each site (94 bulk SOC and 94 PyC_{HyPy} samples). Total SOC contents decreased rapidly to <0.4% with soil depth >15 cm for most of the southern sites[23], which did not allow a sufficient extraction of PyC_{HyPy} in quantities that would produce sufficient CO_2 for a robust ^{14}C measurement. Deeper analyses to 60 cm soil depth were performed for sites N2 and N5 (29 bulk and 16 PyC_{HyPy} samples), which indicated sufficiently high SOC contents and represented contrasting landscape positions (e.g. N2: lowland and N5: elevated plateau). Samples of PyC_{HyPy} for radiocarbon measurement were isolated from bulk soil as described above, using pre-cleaned quartz HyPy crucibles. After the HyPy procedure, crucibles containing the sample were directly loaded in pre-cleaned quartz combustion tubes. Samples were combusted to produce CO_2, which was then cryogenically purified before being converted to graphite by reduction with Zn and Fe. The $^{14}C/^{12}C$ or $^{14}C/^{13}C$ ratio of sample graphite was measured using accelerator mass spectrometry at the Scottish Universities Environmental Research Centre (SUERC) AMS facility, or the Keck Carbon Cycle Accelerator Facility at the University of California, Irvine. For samples generating >500 µg C for measurement, an aliquot of CO_2 was used to measure $\delta^{13}C$ for normalization of $^{14}C/^{13}C$ ratios. For samples generating <500 µg C for measurement, the $\delta^{13}C$ for normalization was obtained via on-line measurement in the AMS instrument.

For ^{14}C determination of long-chain fatty acids, $C_{28\text{-}30}$ FAMEs were purified using a preparative capillary gas chromatography (PCGC) as described in Feng et al. (ref. 82). In summary, PCGC consisted of a gas chromatograph (GC) system (6890S) coupled to a Gerstel preparative fraction collector (Gerstel PFC) with a VF-1MS column (30 m × 0.53 mm i.d., film thickness, 0.50 µm). Approximately 100 µg carbon of individual compounds were collected after up to 30 injections on the PCGC. A small aliquot of the isolated compounds was used to check purity on a HP 7890 A GC equipped with a flame ionization detector (FID), and a VF-1 MS capillary column (30 m × 0.25 mm, 0.25 µm film thickness). The temperature program started with a 1 min hold time at 50 °C, followed by a 10 °C min^{-1} ramp to 320 °C and a 5 min hold time at 320 °C. All fractions were found to yield purities >99%. Radiocarbon contents of the fatty acids were corrected for derivative carbon (from the methylation). To assess procedural blanks, chemical extraction and PCGC isolation

were carried out with only solvents and reagents, but no sample added. All radiocarbon values are corrected for procedural blanks with the errors propagated.

Individual selected char particles (Supplementary Fig. 2) were washed with deionized water and treated using Acid Base Oxidation-Stepped Combustion using the protocol described by Wood et al. (ref. 83). Fatty acids and individual char particles were analysed at the AMS facility at the Laboratory of Ion Beam Physics at ETH Zurich.

Calculations and statistics

The SOC stocks were corrected for rock and root fragments >2 mm as presented in Schiedung et al. (ref. 23). The PyC contents derived from HyPy (PyC_{HyPy}) and CTO-375 (PyC_{CTO}) contents were calculated as its proportion on total SOC as PyC_{HyPy}/SOC% and PyC_{CTO}/SOC%, respectively. For PyC_{HyPy}/SOC%, the added catalyst was subtracted to obtain the absolute amounts of carbon in the HyPy residue and the initial SOC. The PyC_{HyPy} stocks were calculated by multiplying the PyC_{HyPy}/SOC% with the SOC stocks.

Radiocarbon ages of the PyC_{HyPy} were calibrated with OxCal v4.4.2[84] by using the IntCal20 international northern hemisphere atmosphere calibration curve[85]. All calibrated radiocarbon ages are reported at two sigma (95%) confidence (e.g. min. and max. age) relative to AD 1950 (=0 before present, BP) and expressed as cal. yrs BP.

Differences in contents and stocks of PyC_{HyPy} and SOC within northern and southern sites were tested using analysis of variances (ANOVA). Multiple comparison with a post-hoc-test (Tukey; 95% pairwise confidence level) and Bonferroni adjustment was conducted to compute *p*-values using the *multcomp* package[86]. Student's *t* tests (two-sided) were computed to test significant differences between aggregated values of northern and southern sites. Normal distribution and homogeneity of variances were tested using Shapiro–Wilk and Levene's tests and log-transformation was used to fulfil criteria if needed. Two-sample Wilcox test was used to test differences between PyC_{HyPy} and Bulk $F^{14}C$ for each site. All values are presented as means per site with the standard error of the mean (SE), if not stated differently.

Drivers of PyC_{HyPy} contents and radiocarbon of PyC_{HyPy} and bulk soil, were determined by considering SOC-specific parameters, soil chemical and composition properties as well es site specific properties, which are described in more detail in Schiedung et al. (ref. 23) and Supplementary Tables 1 and 5. The driver analysis was performed by using site specific values or means of all replicates at each site. Due to the large difference between northern and southern sites in SOC, soil and site properties, non-parametric ranked Kendall correlation analyses were used for driver determination and correlation factors τ were computed with $p < 0.05$ as the significance level. All statistical analyses were performed using R Studio (R Version 4.2.2)[87].

All PyC_{HyPy}, PyC_{CTO} and SOC data from this study is publically available[88].

Reporting summary

Further information on research design is available in the Nature Portfolio Reporting Summary linked to this article.

Data availability

All data presented in this manuscript is available upon request and on Zenodo (https://doi.org/10.5281/zenodo.10037187).

Received: 25 November 2023; Accepted: 25 March 2024;
Published online: 03 April 2024

References

1. Reisser, M., Purves, R. S., Schmidt, M. W. I. & Abiven, S. Pyrogenic carbon in soils: a literature-based inventory and a global estimation of its content in soil organic carbon and stocks. *Front. Earth Sci.* **4**, 1–14 (2016).
2. Santín, C. et al. Towards a global assessment of pyrogenic carbon from vegetation fires. *Glob. Change Biol.* **22**, 76–91 (2016).
3. Bird, M. I. et al. The pyrogenic carbon cycle. *Annu. Rev. Earth Planet. Sci.* **43**, 273–298 (2015).
4. IPCC. Climate Change 2021: The Physical Science Basis. Contribution of Working Group I to the Sixth Assessment Report of the Intergovernmental Panel on Climate Change. In: *Climate Change 2021: The Physical Science Basis. Contribution of Working Group I to the Sixth Assessment Report of the Intergovernmental Panel on Climate Change* (eds. Masson-Delmotte V. et al.) (Cambridge University Press, 2021).
5. Turetsky, M. R. et al. Recent acceleration of biomass burning and carbon losses in Alaskan forests and peatlands. *Nat. Geosci.* **4**, 27–31 (2011).
6. Rogers, B. M., Soja, A. J., Goulden, M. L. & Randerson, J. T. Influence of tree species on continental differences in boreal fires and climate feedbacks. *Nat. Geosci.* **8**, 228–234 (2015).
7. Rantanen, M. et al. The Arctic has warmed nearly four times faster than the globe since 1979. *Commun. Earth Environ.* **3**, 168 (2022).
8. Jones, M. W., Santín, C., van der Werf, G. R. & Doerr, S. H. Global fire emissions buffered by the production of pyrogenic carbon. *Nat. Geosci.* **12**, 742–747 (2019).
9. Bowring, S. P. K. et al. Pyrogenic carbon decomposition critical to resolving fire's role in the Earth system. *Nat. Geosci.* **15**, 135–142 (2022).
10. Schmidt, M. W. I. et al. Persistence of soil organic matter as an ecosystem property. *Nature* **478**, 49–56 (2011).
11. Lehmann, J. et al. Australian climate–carbon cycle feedback reduced by soil black carbon. *Nat. Geosci.* **1**, 832–835 (2008).
12. Schiedung, M. et al. Enhanced loss but limited mobility of pyrogenic and organic matter in continuous permafrost-affected forest soils. *Soil Biol. Biochem.* **178**, 108959 (2023).
13. Wang, J., Xiong, Z. & Kuzyakov, Y. Biochar stability in soil: Meta-analysis of decomposition and priming effects. *GCB Bioenergy* **8**, 512–523 (2016).
14. Lutfalla, S. et al. Pyrogenic carbon lacks long-term persistence in temperate arable soils. *Front. Earth Sci.* **5**, 1–10 (2017).
15. Köchy, M., Hiederer, R. & Freibauer, A. Global distribution of soil organic carbon—Part 1: Masses and frequency distributions of SOC stocks for the tropics, permafrost regions, wetlands, and the world. *Soil* **1**, 351–365 (2015).
16. Jackson, R. B. et al. The ecology of soil carbon: pools, vulnerabilities, and biotic and abiotic controls. *Annu. Rev. Ecol. Evol. Systematics* **48**, 419–445 (2017).
17. Hugelius, G. et al. Large stocks of peatland carbon and nitrogen are vulnerable to permafrost thaw. *Proc. Natl Acad. Sci. USA* **117**, 20438–20446 (2020).
18. Schuur, E. A. G. et al. Climate change and the permafrost carbon feedback. *Nature* **520**, 171–179 (2015).
19. Turetsky, M. R. et al. Carbon release through abrupt permafrost thaw. *Nat. Geosci.* **13**, 138–143 (2020).
20. Hobbie, S. E., Schimel, J. P., Trumbore, S. E. & Randerson, J. R. Controls over carbon storage and turnover in high-latitude soils: Carbon storage and turnover in northern soils. *Glob. Change Biol.* **6**, 196–210 (2000).
21. Deluca, T. H. & Boisvenue, C. Boreal forest soil carbon: distribution, function and modelling. *Forestry* **85**, 161–184 (2012).
22. Chai, X., Li, G., Shi, Z. & Ruan, H. Soil radiocarbon abundance in global forest ecosystems controlled by climate and soil properties. *Plant Soil* **489**, 125–137 (2023).
23. Schiedung, M., Bellè, S.-L., Malhotra, A. & Abiven, S. Organic carbon stocks, quality and prediction in permafrost-affected forest soils in North Canada. *CATENA* **213**, 106194 (2022).
24. Ping, C. L. et al. Permafrost soils and carbon cycling. *Soil* **1**, 147–171 (2015).

25. Schwab, M. S. et al. An abrupt aging of dissolved organic carbon in large arctic rivers. *Geophys Res Lett* **47**, e2020GL088823 (2020).
26. Estop-Aragonés, C. et al. Assessing the potential for mobilization of old soil carbon after permafrost thaw: a synthesis of ^{14}C measurements from the northern permafrost region. *Glob. Biogeochem. Cycles* **34**, e2020GB006672 (2020).
27. Goñi, M. A., Yunker, M. B., Macdonald, R. W. & Eglinton, T. I. The supply and preservation of ancient and modern components of organic carbon in the Canadian Beaufort Shelf of the Arctic Ocean. *Marine Chemistry* **93**, 53–73 (2005).
28. Hilton, R. G. et al. Erosion of organic carbon in the Arctic as a geological carbon dioxide sink. *Nature* **524**, 84–87 (2015).
29. Campeau, A. et al. Controls on the 14C content of dissolved and particulate organic carbon mobilized across the Mackenzie River Basin, Canada. *Glob. Biogeochem. Cycles* **34**, e2020GB006671 (2020).
30. Bröder, L. et al. Preferential export of permafrost-derived organic matter as retrogressive thaw slumping intensifies. *Environ. Res. Lett.* **16**, 054059 (2021).
31. Guggenberger, G. et al. Storage and mobility of black carbon in permafrost soils of the forest tundra ecotone in Northern Siberia. *Glob. Change Biol.* **14**, 1367–1381 (2008).
32. Kane, E. S. et al. Topographic controls on black carbon accumulation in Alaskan black spruce forest soils: implications for organic matter dynamics. *Biogeochemistry* **100**, 39–56 (2010).
33. Rodionow, A., Flessa, H., Kazansky, O. & Guggenberger, G. Organic matter composition and potential trace gas production of permafrost soils in the forest tundra in northern Siberia. *Geoderma* **135**, 49–62 (2006).
34. Schmidt, M. W. I., Skjemstad, J. O., Czimczik, C. I. & Prentice, K. M. Comparative analysis of black carbon in soils. *Glob. Biogeochem. Cycles* **15**, 163–167 (2001).
35. Hammes, K. et al. Comparison of quantification methods to measure fire-derived (black-elemental) carbon in soils and sediments using reference materials from soil, water, sediment and the atmosphere. *Global Biogeochemical Cycles* **21**. https://doi.org/10.1029/2006GB002914 (2007).
36. Zimmerman, A. R. & Mitra, S. Trial by fire: on the terminology and methods used in pyrogenic organic carbon research. *Front. Earth Sci.* **5**. https://doi.org/10.3389/feart.2017.00095 (2017).
37. Krull, E. S., Swanston, C. W., Skjemstad, J. O. & McGowan, J. A. Importance of charcoal in determining the age and chemistry of organic carbon in surface soils: Charcoal chhemistry and age. *J. Geophys. Res.* **111**. https://doi.org/10.1029/2006JG000194 (2006).
38. Preston, C. M. et al. Charcoal in organic horizon and surface mineral soil in a boreal forest fire chronosequence of Western Quebec: stocks, depth distribution, chemical properties and a synthesis of related studies. *Front. Earth Sci.* **5**, 1–20 (2017).
39. Schmidt, M. W. I., Skjemstad, J. O. & Jäger, C. Carbon isotope geochemistry and nanomorphology of soil black carbon: Black chernozemic soils in central Europe originate from ancient biomass burning. *Glob. Biogeochem. Cycles* **16**, 70-1–70–8 (2002).
40. Hammes, K., Torn, M. S., Lapenas, A. G. & Schmidt, M. W. I. Centennial black carbon turnover observed in a Russian steppe soil. *Biogeosciences* **5**, 1339–1350 (2008).
41. Leifeld, J., Heiling, M. & Hajdas, I. Age and thermal stability of particulate organic matter fractions indicate the presence of black carbon in soil. *Radiocarbon* **57**, 99–107 (2015).
42. Coppola, A. I. et al. The black carbon cycle and its role in the Earth system. *Nat. Rev. Earth Environ.* https://doi.org/10.1038/s43017-022-00316-6 (2022).
43. Jones, M. W. et al. Fires prime terrestrial organic carbon for riverine export to the global oceans. *Nat. Commun.* **11**, 2791 (2020).
44. Ziolkowski, L. A. & Druffel, E. R. M. Aged black carbon identified in marine dissolved organic carbon. *Geophy. Res. Lett.* **37**, 4–7 (2010).
45. Bostick, K. W. et al. Production and composition of pyrogenic dissolved organic matter from a logical series of laboratory-generated chars. *Front. Earth Sci.* **6**, 1–14 (2018).
46. Eckdahl, J. A. et al. Mineral soils are an important intermediate storage pool of black carbon in Fennoscandian Boreal Forests. *Glob. Biogeochem. Cycles* **36**, 1–16 (2022).
47. Ascough, P. L. et al. Hydropyrolysis as a new tool for radiocarbon pretreatment and the quantification of black carbon. *Quaternary Geochronol.* **4**, 140–147 (2009).
48. Meredith, W. et al. Assessment of hydropyrolysis as a method for the quantification of black carbon using standard reference materials. *Geochim. Cosmochim. Acta* **97**, 131–147 (2012).
49. Trumbore, S. Radiocarbon and soil carbon dynamics. *Annu. Rev. Earth Planet. Sci.* **37**, 47–66 (2009).
50. Mueller, C. W. et al. Large amounts of labile organic carbon in permafrost soils of northern Alaska. *Glob. Change Biol.* **21**, 2804–2817 (2015).
51. Zimov, S. A. Permafrost and the global carbon budget. *Science* **312**, 1612–1613 (2006).
52. Dalton, A. S. et al. An updated radiocarbon-based ice margin chronology for the last deglaciation of the North American ice sheet complex. *Quat. Sci. Rev.* **234**, 1–27 (2020).
53. Smith, D. G. Glacial Lake McConnell: Paleogeography, age, duration, and associated river deltas, Mackenzie River basin, western Canada. *Quat. Sci. Rev.* **13**, 829–843 (1994).
54. Andreev, A. A. et al. Vegetation and climate history in the Laptev Sea region (Arctic Siberia) during Late Quaternary inferred from pollen records. *Quat. Sci. Rev.* **30**, 2182–2199 (2011).
55. Zimmermann, H. et al. The History of Tree and Shrub Taxa on Bol'shoy Lyakhovsky Island (New Siberian Archipelago) since the Last Interglacial Uncovered by Sedimentary Ancient DNA and Pollen Data. *Genes* **8**, 273 (2017).
56. Anderson, R. S. et al. Holocene development of Boreal forests and fire regimes on the Kenai Lowlands of Alaska. *Holocene* **16**, 791–803 (2006).
57. Remy, C. C. et al. Climatic and vegetational controls of Holocene wildfire regimes in the boreal forest of northern Fennoscandia. *J. Ecol.* **111**, 845–860 (2023).
58. Hudspith, V. A., Belcher, C. M., Kelly, R. & Hu, F. S. Charcoal reflectance reveals early Holocene Boreal Deciduous Forests burned at high intensities. *PLoS ONE* **10**, e0120835 (2015).
59. Schiedung, M. et al. Vertical mobility of pyrogenic organic matter in soils: a column experiment. *Biogeosciences* **17**, 6457–6474 (2020).
60. Soucémarianadin, L. N., Quideau, S. A. & MacKenzie, M. D. Pyrogenic carbon stocks and storage mechanisms in podzolic soils of fire-affected Quebec black spruce forests. *Geoderma* **217–218**, 118–128 (2014).
61. Soucémarianadin, L. et al. Pyrogenic carbon content and dynamics in top and subsoil of French forests. *Soil Biol. Biochem.* **133**, 12–15 (2019).
62. Yunker, M. B. et al. Sources and significance of alkane and PAH hydrocarbons in Canadian Arctic Rivers. *Estuarine Coast. Shelf Sci.* **55**, 1–31 (2002).
63. Kabanov, P. & Gouwy, S. A. The Devonian Horn River Group and the basal Imperial Formation of the central Mackenzie Plain, N.W.T., Canada: multiproxy stratigraphic framework of a black shale basin. *Can J. Earth Sci.* **54**, 409–429 (2017).
64. Volkman, J. K. et al. Microalgal biomarkers: a review of recent research developments. *Organic Geochem.* **29**, 1163–1179 (1998).
65. Kalks, F. et al. Geogenic organic carbon in terrestrial sediments and its contribution to total soil carbon. *SOIL* **7**, 347–362 (2021).
66. Lantz, T. C. & Kokelj, S. V. Increasing rates of retrogressive thaw slump activity in the Mackenzie Delta region, N.W.T., Canada. *Geophys. Res. Lett.* **35**, 2007GL032433 (2008).

67. Vonk, J. E. et al. Spatial variations in geochemical characteristics of the modern Mackenzie Delta sedimentary system. *Geochim. Cosmochim. Acta* **171**, 100–120 (2015).
68. Coppola, A. I. et al. Global-scale evidence for the refractory nature of riverine black carbon. *Nat. Geosci.* **11**, 584–588 (2018).
69. Kane, E. S. et al. Topographic influences on wildfire consumption of soil organic carbon in interior Alaska: Implications for black carbon accumulation. *J. Geophys. Res.* **112**, G03017 (2007).
70. Brodowski, S., Amelung, W., Haumaier, L. & Zech, W. Black carbon contribution to stable humus in German arable soils. *Geoderma* **139**, 220–228 (2007).
71. Major, J., Lehmann, J., Rondon, M. & Goodale, C. Fate of soil-applied black carbon: Downward migration, leaching and soil respiration. *Glob. Change Biol.* **16**, 1366–1379 (2010).
72. Strauss, J. et al. The deep permafrost carbon pool of the Yedoma region in Siberia and Alaska. *Geophys. Res. Lett.* **40**, 6165–6170 (2013).
73. Walker, X. J. et al. Soil organic layer combustion in boreal black spruce and jack pine stands of the Northwest Territories, Canada. *Int. J. Wildland Fire* **27**, 125–134 (2018).
74. Burgeon, V. et al. Organo-mineral associations largely contribute to the stabilization of century-old pyrogenic organic matter in cropland soils. *Geoderma* **388**, 114841 (2021).
75. Brodowski, S., John, B., Flessa, H. & Amelung, W. Aggregate-occluded black carbon in soil. *Eur. J. Soil Sci.* **57**, 539–546 (2006).
76. Pluchon, N. et al. The impact of charcoal and soil mixtures on decomposition and soil microbial communities in boreal forest. *Appl. Soil Ecol.* **99**, 40–50 (2016).
77. Wardle, D. A., Nilsson, M.-C. & Zackrisson, O. Fire-derived charcoal causes loss of Forest Humus. *Science* **320**, 629–629 (2008).
78. Previdi, M., Smith, K. L. & Polvani, L. M. Arctic amplification of climate change: a review of underlying mechanisms. *Environ. Res. Lett.* **16**, 093003 (2021).
79. Walthert, L. et al. Determination of organic and inorganic carbon, δ^{13}C, and nitrogen in soils containing carbonates after acid fumigation with HCl. *J. Plant Nutrition Soil Sci.* **173**, 207–216 (2010).
80. Agarwal, T. & Bucheli, T. D. Adaptation, validation and application of the chemo-thermal oxidation method to quantify black carbon in soils. *Environ. Pollution* **159**, 532–538 (2011).
81. Lattaud, J. et al. Influence of hydraulic connectivity on carbon burial efficiency in Mackenzie Delta Lake sediments. *JGR Biogeosci.* **126**, e2020JG006054 (2021).
82. Feng, X. et al. 14C and 13C characteristics of higher plant biomarkers in Washington margin surface sediments. *Geochim. Cosmochim. Acta* **105**, 14–30 (2013).
83. Wood, R. E. et al. Testing the ABOx-SC method: Dating known-age charcoals associated with the Campanian Ignimbrite. *Quat. Geochronol.* **9**, 16–26 (2012).
84. Bronk Ramsey C. OxCal v4.4.2. https://c14.arch.ox.ac.uk/oxcal.html (2020).
85. Reimer, P. J. et al. The IntCal20 Northern Hemisphere radiocarbon age calibration curve (0-55 cal kBP). *Radiocarbon* **62**, 725–757 (2020).
86. Hothorn, T. et al. Multcomp package: Simultaneous inference in general parametric models (Version1.4-17) (2021).
87. R Core Team. *R: A Language and Environment for Statistical Computing* (R Foundation for Statistical Computing, 2022).
88. Schiedung, M., & Abiven, S. Dataset to Schiedung et al. (2024): Millennial-aged pyrogenic carbon in high-latitude mineral soils. https://doi.org/10.5281/zenodo.10037187 (2024).
89. Gruber, S. Derivation and analysis of a high-resolution estimate of global permafrost zonation. *Cryosphere* **6**, 221–233 (2012).
90. Whiticar, M. J. Stable isotope geochemistry of coals, humic kerogens and related natural gases. *Int. J. Coal Geol.* **32**, 191–215 (1996).
91. Johnstone, J. F. & Hollingsworth, T. N. Chapin III F. S. A key for predicting postfire successional trajectories in black spruce stands of interior Alaska. U.S. Department of Agriculture, Forest Service, Pacific Northwest Research Station, Portland, OR. https://doi.org/10.2737/PNW-GTR-767 (2008).

Acknowledgements

This work was funded by the Swiss National Science Foundation (project no. 200021_178768) and conducted under a Northwest Territories Scientific Research Licence (licence no. 16550). We thank the Community of the Northwest Territory M´etis Nation (Fort Smith), the Aurora Research Institute and Wood Buffalo National Park for support during fieldwork. We thank the CEREEP-Ecotron Ile De France, ENS, CNRS, PSL University, St-Pierre-lès-Nemours, France. J.L. was funded by a Rubicon grant (019.183EN.002) from Netherlands Organization for scientific research. For support of radiocarbon analysis, we thank Thomas Keller and Markus Egli (University of Zurich) for analysing char particles and Richard Staff (NERC Radiocarbon Facility) for support during calibration of radiocarbon ages. We thank the soil organic matter research group at the Thünen Institute of Climate-Smart Agriculture for commenting and discussing previous versions of the manuscript.

Author contributions

S.A. acquired the funding. M.S. and S.A. conceptualized the fieldwork. M.S. and S.-L.B. conducted the fieldwork. M.S., P.A., M.I.B, J.L. and N.H. acquired data. M.S. conducted the data analysis with the contribution of S.A., S.-L.B., P.A., M.I.B., R.G.H., J.L. and L.B. during data interpretation. M.S. wrote the manuscript with the contributions of all authors. The final version of the manuscript was approved by all authors.

Competing interests

The authors declare no competing interests.

Additional information

Supplementary information The online version contains supplementary material available at https://doi.org/10.1038/s43247-024-01343-5.

Correspondence and requests for materials should be addressed to Marcus Schiedung or Samuel Abiven.

Peer review information *Communications Earth and Environment* thanks Si Gao and the other, anonymous, reviewer(s) for their contribution to the peer review of this work. Primary Handling Editors: Yongqiang Liu and Clare Davis. A peer review file is available.